AGU ADVANCING EARTH AND SPACE SCIENCES

Geophysical Research Letters®

RESEARCH LETTER
10.1029/2023GL106840

Observations Reveal Intense Air-Sea Exchanges Over Submesoscale Ocean Front

Haiyuan Yang[1,2], Zhaohui Chen[1,2], Shantong Sun[2], Mingkui Li[1,2], Wenju Cai[1,3], Lixin Wu[1,2], Jinzhuo Cai[1], Bingrong Sun[1], Ke Ma[1], Xiaohui Ma[1,2], Zhao Jing[1,2], and Bolan Gan[1,2]

[1]Frontier Science Center for Deep Ocean Multi-spheres and Earth System (FDOMES) and Physical Oceanography Laboratory, Ocean University of China, Qingdao, China, [2]Laoshan Laboratory, Qingdao, China, [3]State Key Laboratory of Loess and Quaternary Geology, Institute of Earth Environment, Chinese Academy of Sciences, Xi'an, China

Key Points:

- Observations show strong gradient in sea surface temperature and turbulent heat flux across a submesoscale oceanic front
- Submesoscale fronts drive substantially stronger air-sea fluxes and vertical mixing than mesoscale fronts
- The intense air-sea exchanges across submesoscale fronts are not resolved in mesoscale-resolving climate models

Supporting Information:

Supporting Information may be found in the online version of this article.

Correspondence to:

Z. Chen and S. Sun,
chenzhaohui@ouc.edu.cn;
silencesst@gmail.com

Citation:

Yang, H., Chen, Z., Sun, S., Li, M., Cai, W., Wu, L., et al. (2024). Observations reveal intense air-sea exchanges over submesoscale ocean front. *Geophysical Research Letters*, *51*, e2023GL106840. https://doi.org/10.1029/2023GL106840

Received 18 OCT 2023
Accepted 11 JAN 2024

Abstract Air-sea exchanges across oceanic fronts are critical in powering cloud formation, precipitation, and atmospheric storms. Oceanic submesoscale fronts of scales 1–10 km are characterized by strong sea surface temperature (SST) gradients. However, it remains elusive how submesoscale fronts affect the overlying atmosphere due to a lack of high-resolution observations or models. Based on rare high-resolution in situ observations in the Kuroshio Extension region, we quantify the air-sea exchanges across an oceanic submesoscale front. The cross-front SST and turbulent heat flux gradients reaches 2.4°C/km and 47 W/m^2/km, respectively, far stronger than that typically found in mesoscale-resolving products. The stronger SST gradient drives substantially stronger air-sea fluxes and vertical mixing than mesoscale fronts, enhancing cloud formations. The intense air-sea exchanges across submesoscale fronts are confirmed in idealized model simulations, but not resolved in mesoscale-resolving climate models. Our finding provides essential knowledge for improving simulations of cloud formation, precipitation, and storms in climate models.

Plain Language Summary Oceanic fronts, characterized by large sea surface temperature (SST) gradients, are ubiquitous in the global ocean. Through intense heat and moisture release, these oceanic fronts induce large horizontal gradient of sea level pressure or increasing vertical mixing intensity in the lower atmosphere, are critical in powering cloud formation, precipitation, and atmospheric storms, but are sensitive to SST gradients. Oceanic submesoscale fronts of spatial scales 1–10 km are characterized by strong SST gradients. However, our knowledge of how the submesoscale fronts affect the overlying atmosphere is by and large void, due to a lack of high-resolution observations or models. Here, based on high-resolution in situ observations and model simulations, we show that submesoscale fronts drive much stronger air-sea exchanges and vertical mixing as compared to mesoscale fronts, with significant implications for marine atmosphere boundary layer changes and cloud formations. Limited by the coarse resolution, the intense air-sea exchanges across submesoscale fronts are not resolved in mesoscale-resolving climate models. These results highlight the importance of submesoscale air-sea interactions and call for a proper representation of submesoscale air-sea exchanges in the next generation of climate models.

1. Introduction

Oceanic fronts, characterized by large sea surface temperature (SST) gradients, are ubiquitous in the global ocean. Decades of observations and climate modeling studies indicated that oceanic fronts shape the intensity of air-sea fluxes and the movement of overlying atmospheric, especially at mesoscales with cross-front scales from tens to hundreds of kilometers (Czaja et al., 2019; Kelly et al., 2010; Seo et al., 2023; Small et al., 2008). Through intense heat and moisture release, these oceanic fronts impact the overlying atmospheric weathers by strengthening horizontal gradient of sea level pressure (SLP; Lindzen & Nigam, 1987; Mahrt et al., 2004; Minobe et al., 2008; Kawai et al., 2014) or increasing vertical mixing intensity in the lower atmosphere (Chelton et al., 2004; Gan et al., 2023; Hayes et al., 1989; O'Neill et al., 2010; Schneider, 2020; Schneider & Qiu, 2015; Tanimoto et al., 2011; Wallace et al., 1989; Xie, 2004). In response, cross-front variability in local wind and associated vertical motions increase within the marine atmospheric boundary layer (MABL; Chelton et al., 2004; Lindzen & Nigam, 1987; Minobe et al., 2008; O'Neill et al., 2010; Spall, 2007; Tanimoto et al., 2011; Xie, 2004; Small et al., 2019; Strobach et al., 2022; Wallace et al., 1989), which favors cloud formations (Takahashi et al., 2021; Tokinaga et al., 2009; Young & Sikora, 2003) and precipitation (Frenger et al., 2013; Minobe et al., 2008).

Stronger oceanic fronts could intensify extreme atmospheric processes, such as storms (Parfitt & Czaja, 2016; Parfitt et al., 2016), which are sensitive to a space–time alignment between the SST front and storms of similar cross-frontal spatial scales. Air-sea exchanges are mostly active over a narrow space–time scale. When a cold atmosphere meets the warm side of the oceanic fronts, the strong air-sea exchanges enhance precipitation and often facilitate explosive cyclogenesis (Hirata & Nonaka, 2021; Reeder et al., 2021). Atmospheric variability within MABL, in turn, could further drive intense convection into the upper troposphere (Minobe et al., 2008) and excite internal gravity waves that affects the remote atmospheric movements (Kilpatrick et al., 2014; Mahrt et al., 2004).

Failure to resolve the cross-front SST gradient causes large model bias, including the underestimation of climatological convection intensity, cloud formation, and precipitation (Minobe et al., 2008). The underestimated air-sea exchanges due to the unresolved frontal air-sea exchanges also lead to a substantial reduction in the frequency of strong atmospheric fronts (Parfitt et al., 2016) and storm tracks intensity (Kuwano-Yoshida & Minobe, 2017; O'Reilly & Czaja, 2015; O'Reilly et al., 2017).

Compared to mesoscale fronts, SST varies more abruptly across submesoscale fronts of spatial scales 1–10 km, and could potentially exert stronger impacts on the air-sea exchange (Bai et al., 2023; Shao et al., 2019) and atmospheric movement (Chen et al., 2022; Sullivan et al., 2020). However, due to the extremely high resolutions required to resolve submesoscale fronts, only recently have studies started examining the role of submesoscale fronts in regulating the overlying atmospheric activities using observations and idealized models. The rare existing observations on submesoscale air-sea interactions have primarily focused on processes at the air-sea interface and are exclusively located in the low-latitude (Iyer et al., 2022; Shao et al., 2019). Observations of the upper atmospheric responses, particularly the responses of MABL, are still missing in the mid-latitude regions. The existing model studies are highly ideal without discussions associated atmospheric humidity, which is essential for cloud formation and precipitation (Chen et al., 2022; Sullivan et al., 2020; Wenegrat & Arthur, 2018). Thus, it remains elusive as to what the amplitude of the exchange is, or how deep the submesdoscale fronts affect the overlying atmosphere.

Here, based on high-resolution in situ observations and model simulations, we show that submesoscale fronts drive much stronger air-sea exchanges and vertical mixing, with significant implications for MABL changes and cloud formations, as compared to mesoscale fronts. This is, to our knowledge, the first direct field observations of submesoscale air-sea interactions in the mid-latitude region.

2. Intense Air-Sea Exchanges Across the Submesoscale Front in Observations

2.1. In Situ Observations in the Kuroshio-Oyashio Extension

On 10 April 2016, we carried out a transect across a submesoscale front at the northern edge of a warm eddy, which was shed from the northward-intruding Kuroshio-Oyashio Extension meandering (Figure 1a). High-resolution hydrographical and meteorological measurements were made along the transect (Figures S1a and S1b and Table S1 in Supporting Information S1) to obtain the structure of the submesoscale front and examine its impacts on the overlying atmosphere. In the ocean, SST is obtained from a shipboard temperature recorder; temperature and salinity fields below the sea surface are measured with the expendable conductivity-temperature-depth (XCTD) system; and horizontal velocity is obtained from shipboard acoustic Doppler current profilers (ADCP). In the atmosphere, the cloud base is derived from ceilometer; surface air temperature, local SLP, and surface wind are measured by the vessel monitoring system (VMS); wind velocity, air pressure, and air temperature in the upper atmosphere are obtained from Global Position System (GPS) radiosondes (Text S1 in Supporting Information S1). During the shipboard observation period, there is a prevailing northerly wind of ∼7 m/s, which gradually turns westward with height (Table S2 in Supporting Information S1). The oceanic front is also approximately steady without significant changes.

2.2. Air-Sea Exchanges Across the Submesoscale Front

The submesoscale front is characterized by a strong SST gradient that is 3–10 times larger than that typically found in satellite observation and mesoscale-resolving models (Figures 1b and 1c). Across the front in less than 10 km, the surface temperature changes by 12°C with maximum cross-front SST gradient reaches 2.4 C km^{-1}

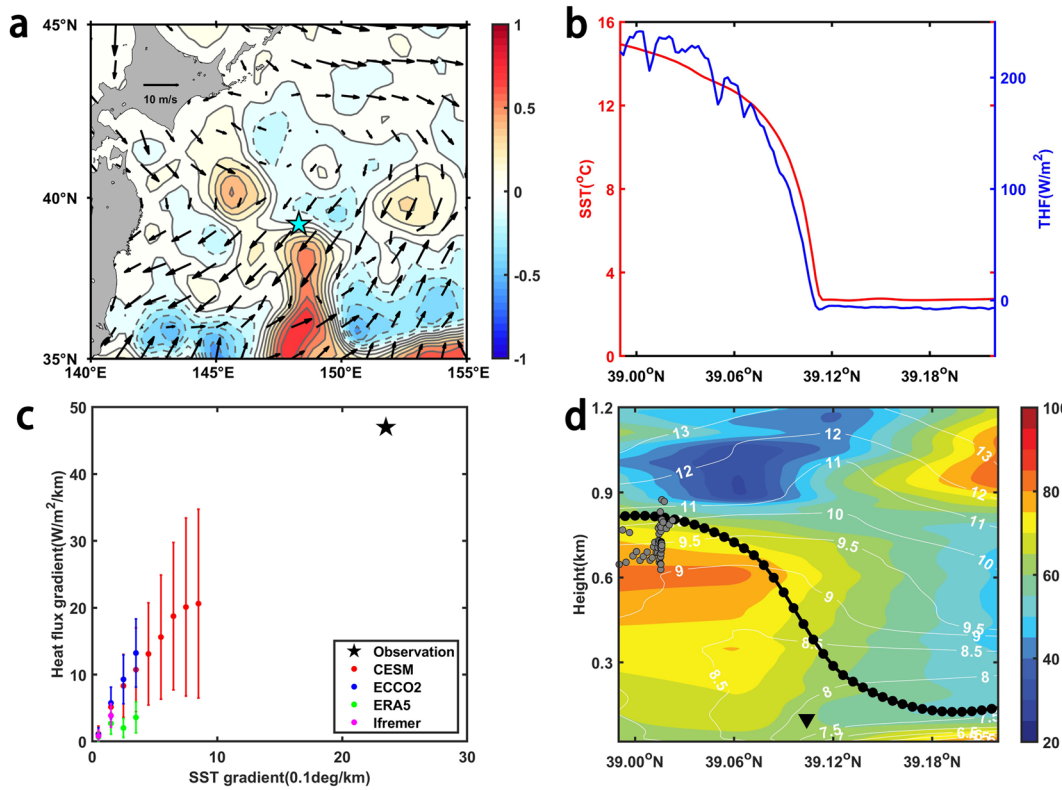

Figure 1. Observed atmosphere response to submesoscale front. (a) Sea surface height anomaly field (shading) and surface wind (vector). (b) SST (red) and THF (blue) across the front. (c) Comparison of the SST gradient and heat flux gradient from observation and other products. The SST and heat flux gradients in observations are calculated based on the average between 39.08°N and 39.11°N. The error bars indicate the standard deviation. (d) Relative humidity (%; shading), potential temperature (°C; contour), MABL (black dotted line) and cloud base (gray dots). The black triangle denotes the position of front. Observations reveal large SST and THF gradients across the submesoscale front, which are not resolved in the widely used data and drive a strong cross-front gradient in the MABL.

(Figure 1b). A strong meridional buoyancy gradient across the front favors the development of submesoscale variability (Text S2 and Figures S1c–S1e in Supporting Information S1). Due to the strong SST gradient, both the air-sea temperature contrast and atmospheric stability are substantially different across the front. From the cold side southward across the front within 5 km, surface air temperature (SAT) increases by 4°C, the upward turbulent heat flux (THF; Text S3 in Supporting Information S1) increases by 200 W/m^2, and surface wind speed changes by 3 m/s (Figure 1b and Figures S2a and S2b in Supporting Information S1). The sharp cross-front change in air-sea flux and surface atmosphere characteristics is in line with previous studies (Bai et al., 2023; Chen et al., 2022). In contrast to these abrupt changes, SLP decreases gradually by only 3 hPa across the front (Figure S2a in Supporting Information S1). The cross-front changes in surface properties also lead to a convergence in surface wind stress (Text S4 and Figure S2b in Supporting Information S1), qualitatively consistent with previous observations of mesoscale fronts (Chelton et al., 2004; Xie, 2004).

Our observations reveal abrupt changes in air-sea exchanges across the submesoscale front with maximum cross-front THF gradient reaching ~47 W/m^2 km^{-1}, which is more than 1.5 times larger than the widely used mesoscale eddy-resolving/eddy-permitting satellite observations, reanalysis data, and model products (Figure 1c; Text S5 in Supporting Information S1). Similarly, the surface drag coefficient also depicts a much larger cross-front change than previous theorical estimation for mesoscale front (Text S6 and Figure S3 in Supporting Information S1; Kudryavtsev et al., 2005). The prominent cross-front variability in air-sea exchange leaves footprints on the MABL convergence (Figure 1d). Indeed, the MABL height increases from 150 to 850 m from the cold side southward across the front within 10 km (Text S7 in Supporting Information S1). This change in the MABL height is comparable to the MABL height changes above major western boundary currents over tens to hundreds of kilometers (Minobe et al., 2008; Strobach et al., 2022), indicating that the MABL height gradient in

our observations are several times stronger. The higher MABL is also accompanied with an increase in potential temperature and relative humidity on the warm side of the front. Critically, the higher relative humidity is detected just beneath the upper boundary of the MABL on the warm side, leading to a lower cloud base. The cloud base is at around above 3,500 m height on the cold side of the front but decreases to 700 m height on the warm side (black dotted line in Figure 1d). There is also a front-induced secondary circulation in latitude-height space (Kilpatrick et al., 2014; Sullivan et al., 2020; Wai & Stage, 1989). Above the submesoscale front, we observe a strong wind divergence close to the sea surface, which is associated with a downdraft of order 0.1 m/s above the submesoscale front (Figure S2c and Text S4 in Supporting Information S1). Same as the surface fluxes, the observed MABL changes and the wind divergence/downdraft velocity are also much stronger than those reported for mesoscale fronts of similar cross-front SST contrasts (cyaneous lines in Figure S2c in Supporting Information S1; Minobe et al., 2008; Tokinaga et al., 2009; O'Neill et al., 2017; Strobach et al., 2022).

Additionally, the gradual cross-front changes in SLP suggest that the pressure adjustment may play a less important role in submesoscale air-sea interactions, as compared to mesoscale air-sea interactions (Gan et al., 2023; Minobe et al., 2008). In the next section, we will compare the different processes involved in submesoscale and mesoscale air-sea interactions using an SST-forced atmospheric model.

3. Stronger Air-Sea Exchange Across Submesoscale Fronts Than Mesoscale Fronts

3.1. Model Configurations

To highlight the differences between submesoscale and mesoscale air-sea interactions, we conduct a set of simulations based on Weather Research and Forecasting Model (WRF; Text S8 and Figure S4 in Supporting Information S1). The WRF model is developed by the National Center for Atmospheric Research and is configured on Arakawa-C grid at 1-km horizontal resolution with 30 vertical levels. The model output is saved every 3 hr. The model domain is 800 km × 800 km (Figure S4 in Supporting Information S1) and the bottom boundary condition is an idealized oceanic front that separates two regions of uniform SST, 4°C and 15°C (Figure S4a in Supporting Information S1). The initial and lateral boundary conditions are area- and time-mean values derived from ERA5 data over 36–44°N, 146–154°E during December, 2015. In particular, the initial wind velocity is northly, and the bottom boundary condition is an idealized oceanic front that separates two regions of uniform SST, 4°C and 15°C (Figure S4a in Supporting Information S1). During the model runs, both the lateral and bottom boundary conditions are kept constant.

Two atmospheric simulations are conducted: submesoscale front-driven experiment (SubMesoF) and mesoscale front-driven experiment (MesoF). In SubMesoF, the SST increases across the front from 4°C to 15°C in 4 km, close to the observation (Figure 3a). In comparison, the cross-front SST increase occurs over 40 km in MesoF (Figure 3a), comparable to the maximum SST gradient in satellite observation (Figure 1c). As such, a comparison between them allows us to compare the impacts of oceanic submesoscale and mesoscale fronts on the overlying air. Both SubMesoF and MesoF reach steady states in 9 hr, judged by changes in the total kinetic energy, and the data from model day 3–10 are used for analysis.

The SubMesoF, largely reproduces the observed atmospheric activities above the submesoscale front, including the sharp changes in wind field, surface air temperature and surface fluxes, and the gradual cross-front changes in SLP (Figures S5a–S5c in Supporting Information S1). Within the MABL, the cross-front change in the MABL height, the magnitude of wind divergence and vertical velocity, and the formation of cloud are also qualitatively close to observations (Figures S5d–S5f in Supporting Information S1).

3.2. Air-Sea Exchange Across Submesoscale Fronts Versus Mesoscale Fronts

The submesoscale front appears to drive stronger air-sea fluxes than the mesoscale front. In comparison with submesoscale air-sea interactions, the weaker SST gradient in MesoF leads to more gradual changes in surface fluxes (Figure 2b and Figure S6a in Supporting Information S1). When integrated over the frontal region (39.8°N–40.2°N), the surface heat and moisture fluxes in MesoF are about 20% smaller than SubMesoF. This enhanced air-sea flux above the submesoscale front, consistent with previous studies (Bai et al., 2023; Chen et al., 2022; Strobach et al., 2022), is mainly associated with a stronger vertical mixing (Figure 2c and Figure S6b in Supporting Information S1). Here we take the surface heat flux as an example to explain the reasons.

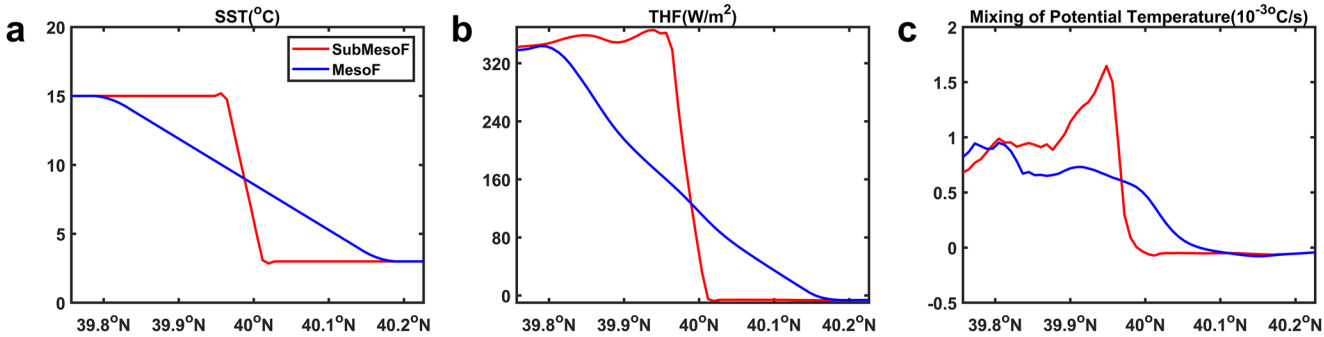

Figure 2. Atmosphere response to submesoscale front versus to mesoscale front at sea surface. (a) SST across the front in SubMesoF (red) and MesoF (blue). (b) THF. (c) Mixing of potential temperature. Compared to the mesoscale front, submesoscale front induces a larger gradient of air-sea heat exchanges and more intense mixing across the submesoscale front.

Differences in the surface heat flux between SubMesoF and MesoF are dominated by latent heat flux changes. The surface latent heat flux is determined by the surface wind speed (U_a), surface specific humidity (q), saturation specific humidity (q_s), and the air-sea transfer coefficient (C_h; Figure S7 in Supporting Information S1; Fairall et al., 2003). Southward across the front, the abrupt change in the air-sea temperature difference destabilizes the atmosphere and leads to a larger heat release and stronger mixing on the warm side of the submesoscale front. This enhanced mixing causes the air-sea transfer coefficient to peak just on the southern edge of the submesoscale front (Figure S7 in Supporting Information S1). In comparison, the mesoscale front forces a more gradual cross-front change in the atmosphere.

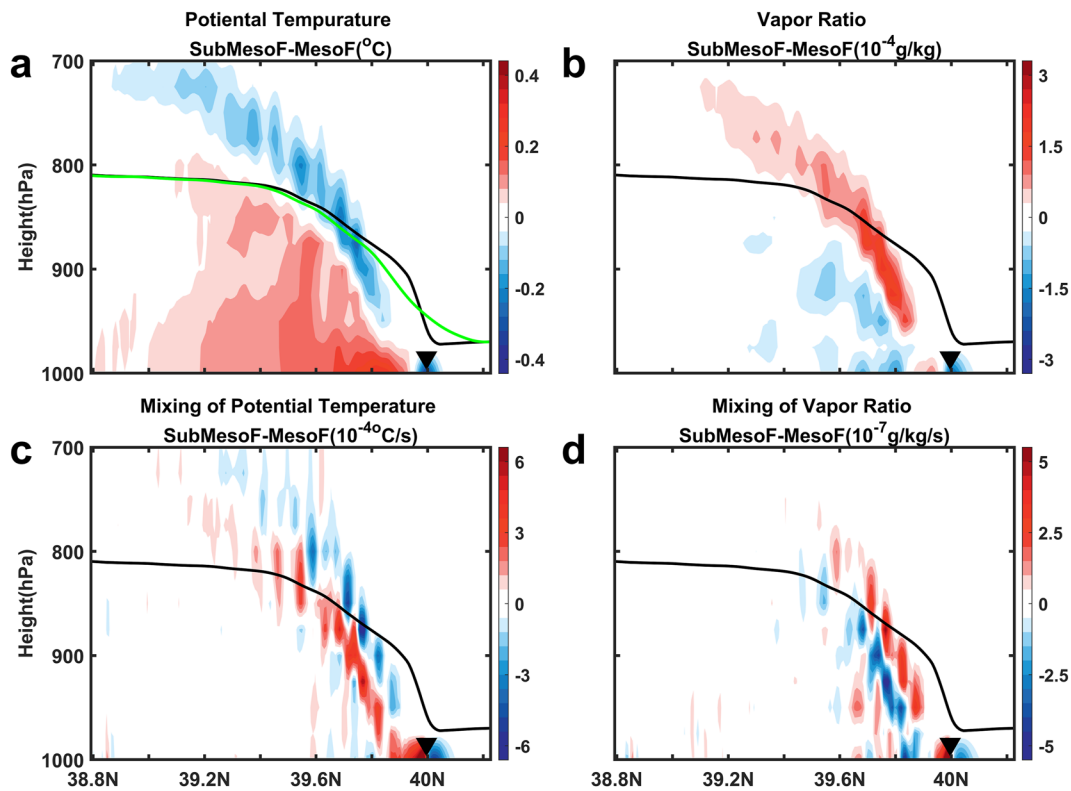

Figure 3. Atmosphere response to submesoscale front versus to mesoscale front in the MABL. (a) Potential temperature difference (SubMesoF-MesoF). The black (green) line depicts the MABL height in SubMesoF (MesoF) and the black triangle denotes the position of front. (b) Vapor ratio difference. (c) Difference of potential temperature mixing. (d) Difference of vapor ratio mixing. Submesoscale front induces a more intense atmosphere response in the vicinity of MABL, as compared to the mesoscale front.

To confirm the mechanism that accounts for the different atmospheric responses, a budget analysis at 1000 hPa is conducted (Text S9 and Figure S8 in Supporting Information S1). For potential temperature and water vapor ratio, the results suggest an evolving balance between advection and mixing. The sign of the mixing term is positive as the wind pass the SST front, suggesting that the ocean moistens and heats the atmosphere, consistent with the patterns of surface fluxes (Figure 2 and Figure S6 in Supporting Information S1). Similarly, the cross-front variation of v budget shows a primary balance between mixing and advection as well, whereas the contributions from the pressure gradient and the Coriolis terms are secondary. The relative importance of pressure adjustment and mixing could also be understood based on scale analysis (Ayet & Redelsperger, 2019, Equation 21 in their paper). Compared to that in MesoF, front in SubMesoF is characterized by a much larger SST gradient, that is, $\Delta SST/\Delta L$ with L indicating cross-front scale. As a result, the magnitude of mixing (in direct proportion to $\Delta SST/\Delta L$; second term in their Equation 21) and its role in regulating wind field is much larger in SubMesoF. The comparison between SubMesoF and MesoF suggest that the different mixing strength account for the different atmospheric responses between submesoscale and mesoscale fronts.

The impact of submesoscale fronts extends beyond the sea surface as in observations with an abrupt lifting of the MABL height within 10 km (black line in Figure 3a). The potential temperature (Figure S9a in Supporting Information S1) and water vapor (Figure S9b in Supporting Information S1) depicts substantial cross-front changes. A lower potential temperature and a higher water vapor are found just beneath the MABL height around 39.6°N–39.9°N (Figures S9and S9b in Supporting Information S1). In comparison with MesoF, the MABL height increases more abruptly in SubMesoF southward across the front (black vs. green lines in Figure 3a), accompanied by significant differences in potential temperature (Figure 3a) and water vapor (Figure 3b). Within the MABL, the atmospheric potential temperature is higher, and the water vapor ratio is lower in SubMesoF, consistent with the stronger vertical mixing on the warm side of the submesoscale front (Figures 3c and 3d and Figures S9c and S9d in Supporting Information S1).

The mixing-induced temperature and vapor differences between SubMesoF and MesoF could also affect cloud distributions. In SubMesoF, low cloud (formed below 2,000 m or 800 hpa height; black dashed line in) and middle cloud (formed between 2,000 and 6,000 m or 800 hpa–500 hpa height) are found within 39.3°N–39.9°N and south of 39.6°N, respectively (the center of front locates at 40°N; Figures S10a and S10b in Supporting Information S1), consistent with high-level relative humidity and near-zero dew point temperature difference (Figures S11a and S11b in Supporting Information S1). Compared to MesoF, the lower potential temperature and higher vapor ratio (Figures 3a and 3b) close to the upper boundary of the MABL leads to a lower dew temperature and higher relative humidity (Figures S11c and S11d in Supporting Information S1), which favors the formation of cloud. Indeed, we found a significant increase in cloud coverage north of 39.2°N in SubMesoF, mostly located on the warm side of the front (Figures S10c and S10d in Supporting Information S1).

4. Summary and Discussion

The key processes by which a submesoscale front affects the overlying atmospheric activities are summarized in Figure 4. Driven by the intense SST gradient, the gradient in THF is much stronger than that in typical mesoscale-resolving and mesoscale-permitting reanalysis products and models. The strong air-sea flux leads to a far stronger cross-front gradient in the MABL height than previously reported (Minobe et al., 2008; Strobach et al., 2022), along with a larger cloud coverage on the warm side of the front than mesoscales. Besides, the large SST gradient of submesoscale fronts increases the air-sea exchange efficiency and induces a substantially larger THF and moisture flux, compared to the mesoscale fronts.

The intense submesoscale air-sea interaction has profound implications for climate and weather projections. In the presence of submesoscale fronts, the ocean could release more heat and moisture into the atmosphere, which drives stronger local convection systems, including vertical motions, cloud formation and precipitation, that are still challenging to be represented in the mesoscale-resolving climate models (Chang et al., 2020; Small et al., 2019; Yeager et al., 2023; Zhang et al., 2023). Besides, the energetic atmospheric frontal activities and the intensity of storm tracks are fueled by the air-sea interactions in frontal regions (Hirata & Nonaka, 2021; Kuwano-Yoshida & Minobe, 2017; O'Reilly & Czaja, 2015; O'Reilly et al., 2017; Parfitt & Czaja, 2016; Parfitt et al., 2016; Reeder et al., 2021). The missing submesoscale air-sea interactions in climate models could cause an underestimation of those extreme atmospheric events, leading to negative biases in their occurrence and intensity (Parfitt & Czaja, 2016; Parfitt et al., 2016). In addition to facilitating storms, oceanic submesoscale could also

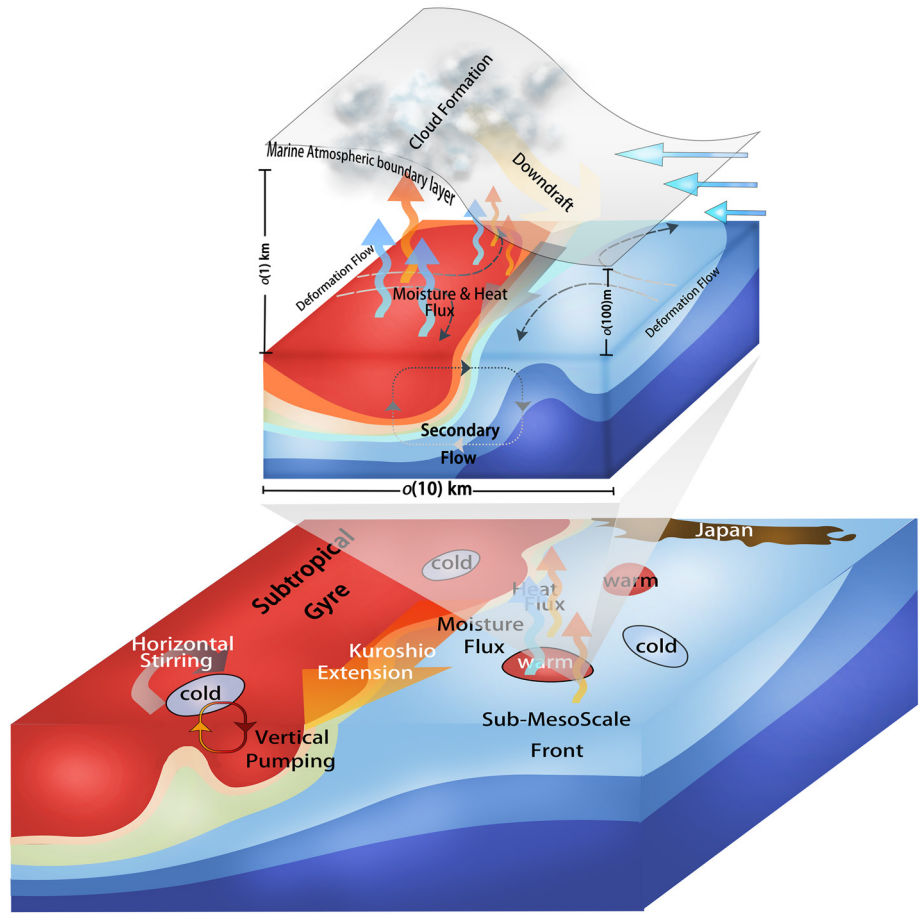

Figure 4. A schematic of the atmospheric responses to an underlying oceanic submesoscale front. With a strong SST gradient, the energetic submesoscale front drives stronger air-sea exchanges as compared to mesoscale fronts. The impact of enhanced air-sea exchanges extends beyond the sea surface, leading to a significant increase in the MABL height and cloud formation on the warm side of the front.

affect weathers after the synoptic processes. For example, the cold wakes left by energetic cyclones are characterized by negative surface heat flux anomalies, a reduction of rainfall and cloud (Ma et al., 2020), and deep mixed layer that favor the formation of oceanic submesoscale (McWilliams, 2016; Taylor & Thompson, 2023). The detailed dynamic processes and role of oceanic submesoscale in this ocean-atmosphere system should be investigate more comprehensively in the future based on high-resolution observations and simulations.

Data Availability Statement

The observation data across the submesoscale front used in this study can be acquired from Yang and Chen (2023). The source code of WRF model is obtained from https://www2.mmm.ucar.edu/wrf/users/download/get_source.html. The sea level height products are distributed by CMEMS and can be download freely after registration from Sea Level Anomaly (2023). The ERA5 products are distributed by ECMWF at Hersbach et al. (2023). The COARE 3.0 algorithm for matlab are freely available at https://www.coaps.fsu.edu/COARE/flux_algor/. Ifrmer and ECCO2 products used in this study can also be obtained from Yang and Chen (2023). The CESM model source code and associated instructions are provided by Laoshan Laboratory and can be downloaded from RUO (2020).

Acknowledgments
We would like to thank all crew of the R/V Dongfanghong 2 for their great efforts. This work was supported by the National Natural Science Foundation of China (42225601) and National Key Research and Development Program of China (2022YFC3104801). H.Y. is partly supported by National Natural Science Foundation of China (42176006) and Z.H. is partly supported by Funds for Leading Talents (2022GJJLJRC02-014). Computation for the work described in this paper was supported by the Marine Big Data Center of Institute for Advanced Ocean Study of Ocean University of China.

References

Ayet, A., & Redelsperger, J.-L. (2019). An analytical study of the atmospheric boundary-layer flow and divergence over an SST front. *Quarterly Journal of the Royal Meteorological Society*, *145*(723), 2549–2567. https://doi.org/10.1002/qj.3578

Bai, Y., Thompson, A., Boas, A., Klein, P., Torres, H., & Menemenlis, D. (2023). Sub-mesoscale wind-front interactions: The combined impact of thermal and current feedback. *Geophysical Research Letters*, *50*(18), e2023GL104807. https://doi.org/10.1029/2023gl104807

Chang, P., Zhang, S., Danabasoglu, G., Yeager, S. G., Fu, H., Wang, H., et al. (2020). An unprecedented set of high-resolution earth system simulations for understanding multiscale interactions in climate variability and change. *Journal of Advances in Modeling Earth Systems*, *12*(12), e2020MS002298. https://doi.org/10.1029/2020ms002298

Chelton, D. B., Schlax, M. G., Freilich, M. H., & Milliff, R. F. (2004). Satellite measurements reveal persistent small-scale features in ocean winds. *Science*, *303*(5660), 978–983. https://doi.org/10.1126/science.1091901

Chen, X., Dewar, W., Chassignet, E., Bourassa, M., Morey, S., & Gopalakrishnan, G. (2022). On the feedback between air-sea turbulent momentum flux and oceanic submesoscale processes. *Journal of Geophysical Research: Oceans*, *127*(10), e2022JC018767. https://doi.org/10.1029/2022jc018767

Czaja, A., Frankignoul, C., Minobe, S., & Vannière, B. (2019). Simulating the midlatitude atmospheric circulation: What might we gain from high-resolution modeling of air-sea interactions? *Current Climate Change Reports*, *5*(4), 390–406. https://doi.org/10.1007/s40641-019-00148-5

Fairall, C. W., Bradley, E. F., Hare, J. E., Grachev, A. A., & Edson, J. B. (2003). Bulk parameterization of air–sea fluxes: Updates and verification for the COARE algorithm. *Journal of Climate*, *16*(4), 571–591. https://doi.org/10.1175/1520-0442(2003)016<0571:bpoasf>2.0.co;2

Frenger, I., Gruber, N., Knutti, R., & Münnich, M. (2013). Imprint of southern ocean eddies on winds, clouds and rainfall. *Nature Geoscience*, *6*(8), 608–612. https://doi.org/10.1038/ngeo1863

Gan, B., Wang, T., Wu, L., Li, J., Qiu, B., Yang, H., & Zhang, L. (2023). A Mesoscale Ocean–atmosphere coupled pathway for decadal variability of the Kuroshio extension system. *Journal of Climate*, *36*(2), 485–510. https://doi.org/10.1175/jcli-d-21-0557.1

Hayes, S., McPhaden, M., & Wallace, J. (1989). The influence of sea surface temperature on surface wind in the eastern equa-torial Pacific. *Journal of Climate*, *2*(12), 1500–1506. https://doi.org/10.1175/1520-0442(1989)002<1500:tiosst>2.0.co;2

Hersbach, H., Bell, B., Berrisford, P., Biavati, G., Horányi, A., Muñoz Sabater, J., et al. (2023). ERA5 hourly data on pressure levels from 1940 to present [Dataset]. Copernicus Climate Change Service (C3S) Climate Data Store (CDS). https://doi.org/10.24381/cds.bd0915c6

Hirata, H., & Nonaka, M. (2021). Impacts of strong warm ocean currents on development of extratropical cyclones through the warm and cold conveyor belts: A review. *Tropical and Extratropical Air-Sea Interactions*, 267–293. https://doi.org/10.1016/b978-0-12-818156-0.00014-9

Iyer, S., Drushka, K., Thompson, E. J., & Thomson, J. (2022). Small-scale spatial variations of air-sea heat, moisture, and buoyancy fluxes in the tropical trade winds. *Journal of Geophysical Research: Oceans*, *127*(10), e2022JC018972. https://doi.org/10.1029/2022jc018972

Kawai, Y., Tomita, H., Cronin, M. F., & Bond, N. A. (2014). Atmospheric pressure response to mesoscale sea surface temperature variations in the Kuroshio Extension region: In situ evidence. *Journal of Geophysical Research: Atmospheres*, *119*(13), 8015–8031. https://doi.org/10.1002/2013jd021126

Kelly, K. A., Small, R. J., Samelson, R. M., Qiu, B., Joyce, T. M., Kwon, Y. O., & Cronin, M. F. (2010). Western boundary currents and frontal air–sea interaction: Gulf Stream and Kuroshio Extension. *Journal of Climate*, *23*(21), 5644–5667. https://doi.org/10.1175/2010jcli3346.1

Kilpatrick, T., Schneider, N., & Qiu, B. (2014). Boundary layer convergence induced by strong winds across a midlatitude SST front. *Journal of Climate*, *27*(4), 1698–1718. https://doi.org/10.1175/jcli-d-13-00101.1

Kudryavtsev, V., Akimov, D., Johannessen, J., & Chapron, B. (2005). On radar imaging of current features: 1. Model and comparison with observations. *Journal of Geophysical Research*, *110*(C7), C07016. https://doi.org/10.1029/2004JC002505

Kuwano-Yoshida, A., & Minobe, S. (2017). Storm-track response to SST fronts in the northwestern Pacific region in an AGCM. *Journal of Climate*, *30*(3), 1081–1102. https://doi.org/10.1175/jcli-d-16-0331.1

Lindzen, R. S., & Nigam, S. (1987). On the role of sea surface temperature gradients in forcing low-level winds and convergence in the tropics. *Journal of the Atmospheric Sciences*, *44*(17), 2418–2436. https://doi.org/10.1175/1520-0469(1987)044<2418:otross>2.0.co;2

Ma, Z., Fei, J., Lin, Y., & Huang, X. (2020). Modulation of clouds andrainfall by tropical cyclone's coldwakes. *Geophysical Research Letters*, *47*(17), e2020GL088873. https://doi.org/10.1029/2020gl088873

Mahrt, L., Vickets, D., & Moore, E. (2004). Flow adjustments across sea-surface temperature changes. *Bound. -Layer Meteor*, *111*(3), 553–564. https://doi.org/10.1023/b:boun.0000016600.63382.5f

McWilliams, J. C. (2016). Submesoscale currents in the ocean. *Proceedings of the Royal Society A: Mathematical, Physical and Engineering Sciences*, *472*(2189), 20160117. https://doi.org/10.1098/rspa.2016.0117

Minobe, S., Kuwano-Yoshida, A., Komori, N., Xie, S. P., & Small, R. J. (2008). Influence of the Gulf Stream on the troposphere. *Nature*, *452*(7184), 206–209. https://doi.org/10.1038/nature06690

O'Neill, L. W., Chelton, D. B., & Esbensen, S. K. (2010). The effects of SST-induced surface wind speed and direction gradients on midlatitude surface vorticity and divergence. *Journal of Climate*, *23*(2), 255–281. https://doi.org/10.1175/2009jcli2613.1

O'Neill, L. W., Haack, T., Chelton, D. B., & Skyllingstad, E. (2017). The Gulf Stream convergence zone in the time-mean winds. *Journal of the Atmospheric Sciences*, *74*(7), 2383–2412. https://doi.org/10.1175/jas-d-16-0213.1

O'Reilly, C. H., & Czaja, A. (2015). The response of the Pacific storm track and atmospheric circulation to Kuroshio Extension variability. *Quarterly Journal of the Royal Meteorological Society*, *141*(686), 52–66. https://doi.org/10.1002/qj.2334

O'Reilly, C. H., Minobe, S., Kuwano-Yoshida, A., & Woollings, T. (2017). The Gulf Stream influence on wintertime North Atlantic jet variability. *Quarterly Journal of the Royal Meteorological Society*, *143*(702), 173–183. https://doi.org/10.1002/qj.2907

Parfitt, R., & Czaja, A. (2016). On the contribution of synoptic transients to the mean atmospheric state in the Gulf Stream region. *Quarterly Journal of the Royal Meteorological Society*, *142*(696), 1554–1561. https://doi.org/10.1002/qj.2689

Parfitt, R., Czaja, A., Minobe, S., & Kuwano-Yoshida, A. (2016). The atmospheric frontal response to SST perturbations in the Gulf Stream region. *Geophysical Research Letters*, *43*(5), 2299–2306. https://doi.org/10.1002/2016gl067723

Reeder, M. J., Spengler, T., & Spensberger, C. (2021). The effect of sea surface temperature fronts on atmospheric frontogenesis. *Journal of the Atmospheric Sciences*, *78*(6), 1753–1771. https://doi.org/10.1175/jas-d-20-0118.1

RUO. (2020). lgan/cesm_sw_1.0.1: Some efforts on refactoring and optimizing the community earth system model (CESM1.3.1) on the Sunway TaihuLight supercomputer (cesm_sw_1.0.1) [Software]. Zenodo. https://doi.org/10.5281/zenodo.3637771

Schneider, N. (2020). Scale and Rossby number dependence of observed wind responses to ocean-mesoscale sea surface temperatures. *Journal of the Atmospheric Sciences*, *77*(9), 3171–3192. https://doi.org/10.1175/jas-d-20-0154.1

Schneider, N., & Qiu, B. (2015). The atmospheric response to weak sea surface temperature fronts. *Journal of the Atmospheric Sciences*, *72*(9), 3356–3377. https://doi.org/10.1175/jas-d-14-0212.1

Sea Level Anomaly. (2023). Global ocean gridded L4 sea surface heights and derived variables reprocessed 1993 ongoing [Dataset]. E.U Copernicus Marine Service Information (CMEMS), Marine Data Store (MDS). https://doi.org/10.48670/moi-00148

Seo, H., O'Neill, L. W., Bourassa, M. A., Czaja, A., Drushka, K., Edson, J. B., et al. (2023). Ocean mesoscale and frontal-scale Ocean–atmosphere interactions and influence on large-scale climate: A review. *Journal of Climate*, *36*(7), 1981–2013. https://doi.org/10.1175/jcli-d-21-0982.1

Shao, M., Ortiz-Suslow, D. G., Haus, B. K., Lund, B., Williams, N. J., Özgökmen, T. M., et al. (2019). The variability of winds and fluxes observed near submesoscale fronts. *Journal of Geophysical Research: Oceans*, *124*(11), 7756–7780. https://doi.org/10.1029/2019jc015236

Small, R. D., de Szoeke, S. P., Xie, S. P., O'neill, L., Seo, H., Song, Q., et al. (2008). Air–sea interaction over ocean fronts and eddies. *Dynamics of Atmospheres and Oceans*, *45*(3–4), 274–319. https://doi.org/10.1016/j.dynatmoce.2008.01.001

Small, R. J., Bryan, F. O., Bishop, S. P., & Tomas, R. A. (2019). Air–sea turbulent heat fluxes in climate models and observational analyses: What drives their variability? *Journal of Climate*, *32*(8), 2397–2421. https://doi.org/10.1175/jcli-d-18-0576.1

Spall, M. A. (2007). Midlatitude wind stress–sea surface temperature coupling in the vicinity of oceanic fronts. *Journal of Climate*, *20*(15), 3785–3801. https://doi.org/10.1175/jcli4234.1

Strobach, E., Klein, P., Molod, A., Fahad, A. A., Trayanov, A., Menemenlis, D., & Torres, H. (2022). Local air-sea interactions at ocean mesoscale and submesoscale in a Western boundary current. *Geophysical Research Letters*, *49*(7), e2021GL097003. https://doi.org/10.1029/2021gl097003

Sullivan, P. P., McWilliams, J. C., Weil, J. C., Patton, E. G., & Fernando, H. J. (2020). Marine boundary layers above heterogeneous SST: Across-front winds. *Journal of the Atmospheric Sciences*, *77*(12), 4251–4275. https://doi.org/10.1175/jas-d-20-0062.1

Takahashi, N., Hayasaka, T., Qiu, B., & Yamaguchi, R. (2021). Observed response of marine boundary layer cloud to the interannual variations of summertime Oyashio extension SST front. *Climate Dynamics*, *56*(11–12), 3511–3526. https://doi.org/10.1007/s00382-021-05649-4

Tanimoto, Y., Kanenari, T., Tokinaga, H., & Xie, S. P. (2011). Sea level pressure minimum along the Kuroshio and its extension. *Journal of Climate*, *24*(16), 4419–4434. https://doi.org/10.1175/2011jcli4062.1

Taylor, J. R., & Thompson, A. F. (2023). Submesoscale dynamics in the upper ocean. *Annual Review of Fluid Mechanics*, *55*(1), 103–127. https://doi.org/10.1146/annurev-fluid-031422-095147

Tokinaga, H., Tanimoto, Y., Xie, S. P., Sampe, T., Tomita, H., & Ichikawa, H. (2009). Ocean frontal effects on the vertical development of clouds over the western North Pacific: In situ and satellite observations. *Journal of Climate*, *22*(16), 4241–4260. https://doi.org/10.1175/2009jcli2763.1

Wai, M. M. K., & Stage, S. A. (1989). Dynamical analyses of marine atmospheric boundary layer structure near the Gulf Stream oceanic front. *Quarterly Journal of the Royal Meteorological Society*, *115*(485), 29–44. https://doi.org/10.1002/qj.49711548503

Wallace, J. M., Mitchell, T. P., & Deser, C. (1989). The influence of sea-surface temperature on surface wind in the eastern equatorial Pacific: Seasonal and interannual variability. *Journal of Climate*, *2*(12), 1492–1499. https://doi.org/10.1175/1520-0442(1989)002<1492:tiosst>2.0.co;2

Wenegrat, J. O., & Arthur, R. S. (2018). Response of the atmospheric boundary layer to submesoscale sea surface temperature fronts. *Geophysical Research Letters*, *45*(24), 13–505. https://doi.org/10.1029/2018gl081034

Xie, S. P. (2004). Satellite observations of cool ocean–atmosphere interaction. *Bulletin of the American Meteorological Society*, *85*(2), 195–208. https://doi.org/10.1175/bams-85-2-195

Yang, H., & Chen, Z. (2023). Dataset for 2023GL106840 [Dataset]. Zenodo. https://doi.org/10.5281/zenodo.10428582

Yeager, S., Danabasoglu, G., Edwards, J., Rosenbloom, N., Castruccio, F., Chang, P., et al. (2023). Bringing the future into focus: Benefits and challenges of high-resolution global climate change simulations. *Computing in Science and Engineering*, *23*(3), 34–41. https://doi.org/10.1109/mcse.2021.3068244

Young, G. S., & Sikora, T. D. (2003). Mesoscale stratocumulus bands caused by Gulf Stream meanders. *Monthly Weather Review*, *131*(9), 2177–2191. https://doi.org/10.1175/1520-0493(2003)131<2177:msbcbg>2.0.co;2

Zhang, S., Xu, S., Fu, H., Wu, L., Liu, Z., Gao, Y., et al. (2023). Toward Earth system modeling with resolved clouds and ocean submesoscales on heterogeneous many-core HPCs. *National Science Review*, *10*(6), nwad069. https://doi.org/10.1093/nsr/nwad069